Sources of Stochasticity in the Growth of Cloud Droplets: Supersaturation Fluctuations versus Turbulent Transport

PRASANTH PRABHAKARAN,[a] SUBIN THOMAS,[a] WILL CANTRELL,[a] RAYMOND A. SHAW,[a] AND FAN YANG[b]

[a] *Department of Physics, Michigan Technological University, Houghton, Michigan*
[b] *Brookhaven National Laboratory, Upton, New York*

(Manuscript received 2 March 2022, in final form 20 July 2022)

ABSTRACT: The role played by fluctuations of supersaturation in the growth of cloud droplets is examined in this study. The stochastic condensation framework and the three regimes of activation of cloud droplets— namely, mean dominant, fluctuation influenced, and fluctuation dominant—are used for analyzing the data from high-resolution large-eddy simulations of the Pi convection-cloud chamber. Based on a detailed budget analysis the significance of all the terms in the evolution of the droplet size distribution equation is evaluated in all three regimes. The analysis indicates that the mean-growth rate is a dominant process in shaping the droplet size distribution in all three regimes. Turbulence introduces two sources of stochasticity, turbulent transport and particle lifetime, and supersaturation fluctuations. The transport of cloud droplets plays an important role in all three regimes, whereas the direct effect of supersaturation fluctuations is primarily related to the activation and growth of the small droplets in the fluctuation-influenced and fluctuation-dominant regimes. We compare our results against the previous studies (experimental and theory) of the Pi chamber, and discuss the limitations of the existing models based on the stochastic condensation framework. Furthermore, we extend the discussion of our results to atmospheric clouds, and in particular focus on recent adiabatic turbulent cloud parcel simulations based on the stochastic condensation framework, and emphasize the importance of entrainment/mixing and turbulent transport in shaping the droplet size distribution.

KEYWORDS: Turbulence; Cloud droplets; Cloud microphysics; Drop size distribution

1. Introduction

Clouds play an important role in Earth's radiation and water budget. The microphysical properties of clouds, which determine their reflectivity and precipitation efficiency, are strongly influenced by the number concentration, size distribution, and chemical composition of the aerosol (Twomey 1977; Albrecht 1989). The interaction between aerosol and cloud properties is considered to be one of the largest uncertainties in Earth's climate projections (Boucher et al. 2013). In this regard, predicting the shape of the droplet size distribution (DSD) under various aerosol and meteorological conditions is key to understanding the behavior of atmospheric clouds.

Traditional uniform condensational growth in an adiabatic cloud parcel results in a narrow cloud droplet size distribution (Yau and Rogers 1996). This is in strong contrast to the broad droplet size distributions obtained from in situ observations (Warner 1969; Paluch and Knight 1984; Desai et al. 2019). Past studies have focused on various mechanisms such as entrainment and mixing (Baker et al. 1980; Telford and Chai 1980; Manton 1979; Paluch and Knight 1986; Yang et al. 2016), stochastic condensation (Cooper 1989; Khvorostyanov and Curry 1999; Lasher-Trapp et al. 2005), Ostwald ripening (Korolev 1995; Yang et al. 2018) and turbulence enhanced collision (Shaw 2003; Grabowski and Wang 2013; Chen et al. 2018) to explain the in situ observations. This article explores the role of turbulent fluctuations on the droplet size distribution in the Pi chamber and in the process assesses the limitations of the parcel approach to cloud microphysics in a turbulent environment. In the Pi chamber, supersaturation fluctuations are a result of turbulent mixing, analogous to the entrainment/mixing process in atmospheric clouds. This makes the Pi chamber an ideal setting to explore the role of supersaturation variability in shaping the DSD.

The concept of stochastic condensation, meaning a fluctuating supersaturation field leads to broadening of cloud droplet size distribution undergoing growth by vapor condensation, was originally proposed in the 1960s (e.g., Mazin 1966). Levin and Sedunov (1966) were apparently the first to write down what can be considered a kinetic equation for stochastic condensation, i.e., an equation for the evolution of the droplet size distribution, and to extend it to the Reynolds-averaged form [e.g., see their Eqs. (1) and (5)]. The development of ideas in stochastic condensation is reviewed by Mazin and Merkulovich (2008), which has an extended English-language summary. What can be considered a general result of the early stochastic condensation literature is that for "adiabatic" conditions, i.e., for a closed parcel, the amount of broadening is minimal, and that some other form of randomness, such as entrainment, transport or variability in time history must be present to produce significant broadening. It is fair to state, however, that when such effects are included it becomes questionable whether the phenomenon should still be referred to as stochastic condensation in the original sense of the phrase.

Prabhakaran's current affiliation: NOAA/Chemical Sciences Laboratory, Boulder, Colorado.

Corresponding author: Prasanth Prabhakaran, prasantp@mtu.edu

DOI: 10.1175/JAS-D-22-0051.1

We recommend the paper by Jeffery et al. (2007) as an excellent overview of stochastic condensation theory and its relation to broader Fokker–Planck approaches.

The idea of stochastic condensation was formalized by Cooper (1989) using a Lagrangian framework and Khvorostyanov and Curry (1999) using an Eulerian framework. Both approaches attempt to capture the different growth histories of cloud droplets growing in a turbulent environment, where the saturation ratio is a fluctuating quantity. The aim is to quantify the broadening of the DSD compared to that obtained from an adiabatic parcel model in which the saturation ratio is uniform throughout the volume of the parcel. Recent numerical simulations (e.g., Paoli and Shariff 2009; Sardina et al. 2015; Siewert et al. 2017; Grabowski and Abade 2017) and experimental studies (Chandrakar et al. 2016) have indicated that supersaturation fluctuations play an important role in the broadening of the DSD. Furthermore, recent studies (Korolev and Mazin 1993; Ditas et al. 2012; Chandrakar et al. 2017; Abade et al. 2018; Prabhakaran et al. 2020; Shawon et al. 2021; Grabowski et al. 2022) have shown that the variability in saturation ratio strongly influences the formation of cloud droplets (i.e., activation of aerosol particles).

Recent experiments in the Michigan Tech Pi chamber coupled with stochastic modeling have implied that turbulent fluctuations in saturation ratio play a prominent role in broadening (increasing numbers of both small and large droplets) the DSD and thus aid in forming droplets that may lead to collision–coalescence (Chandrakar et al. 2016; Desai et al. 2018; Saito et al. 2019; Chandrakar et al. 2020b). In contrast Krueger (2020) argued that the observations from the Pi chamber can be qualitatively reproduced by considering only the mean saturation ratio and size dependent sedimentation effects. In this study, we use large-eddy simulations (LES) of the Pi chamber to understand the role played by supersaturation fluctuations in the growth of cloud droplets. The advantage of the Pi chamber is that we can obtain steady-state conditions (in both experiments and simulations), which considerably simplifies the analysis. Furthermore, due to the limited spatial extent of the simulation domain, we attain a high spatial resolution sufficient to capture the variability in the supersaturation with high accuracy. We use the theoretical framework developed in Prabhakaran et al. (2020) which was used for classifying the activation process into three regimes depending on the magnitude of the mean saturation ratio and its intensity—namely, mean dominant, fluctuation influenced, and fluctuation dominant regimes. A brief outline of this framework is provided in the next section. In section 3, we describe the numerical methodology, which is followed by the results section, and a detailed discussion about previous Pi chamber studies and atmospheric cloud parcel studies.

2. Theory: Reynolds-averaged droplet size distribution evolution equation

In this section, we present the Eulerian framework used for studying the growth of cloud droplets in a turbulent environment. The framework is analogous to the stochastic condensation framework (e.g., Khvorostyanov and Curry 1999), and was recently used for investigating the activation of cloud droplets in a turbulent environment (Prabhakaran et al. 2020). The evolution equation for the droplet size distribution at an Eulerian point $F(r, \mathbf{x})$ (including both activated droplets and hydrated haze droplets) is written as

$$\frac{\partial F}{\partial t} = -\boldsymbol{\nabla}\cdot(F\mathbf{u}) + \frac{\partial}{\partial z}(w_d F) - \frac{\partial}{\partial r}(F\dot{r}) + I\delta(r - r_i, \mathbf{x} - \mathbf{x}_i), \tag{1}$$

where r is the radius of the droplet, $\mathbf{u}$ is the local fluid velocity vector, $w_d(r)$ is the settling velocity of the droplet, $\dot{r}$ is the growth rate of droplets of size r, and I is the injection rate of aerosol of size r_i into a volume of cloud droplets at the location $\mathbf{x}_i$. In a turbulent environment, the instantaneous variables fluctuate. Thus, using Reynolds decomposition, each of these variables can be decomposed into a mean and a fluctuation, represented with an overbar and prime, respectively, e.g., $F = \overline{F} + F'$. Thus, the Reynolds-averaged evolution equation for the size distribution is written as

$$\frac{\partial}{\partial t}(\overline{F}) = -\boldsymbol{\nabla}\cdot(\overline{F}\,\overline{\mathbf{u}}) - \boldsymbol{\nabla}\cdot(\overline{F'\mathbf{u}'}) + \frac{\partial}{\partial z}(w_d\overline{F}) - \frac{\partial}{\partial r}(\overline{F}\,\overline{\dot{r}}) - \frac{\partial}{\partial r}(\overline{F'\dot{r}'}) + I\delta(r - r_i, \mathbf{x} - \mathbf{x}_i). \tag{2}$$

The average of a variable X in the above equation is defined as $\overline{X} = [1/(L_x L_y T_o)]\int\int\int X\,dt\,dx\,dy$, where L_x and L_y represents the horizontal extent of the domain, and T_o is the time window over which the data were sampled. The terms on the right-hand side of Eq. (2) are mean-advective transport, turbulent transport, transport due to settling velocity, growth due to mean saturation ratio, growth due to saturation ratio fluctuations, and the injection/activation rate of aerosol, respectively. Under stationary conditions, $(\partial/\partial t)(\overline{F}) = 0$. Consequently, the terms on the right-hand side of Eq. (2) balance each other such that their net sum is zero. The data analyzed in this study are all in a statistically stationary state, thus allowing this significant simplification. Furthermore, we can make an additional simplification by considering the system to be horizontally homogeneous as we have adiabatic boundary conditions at the lateral boundaries. Please note that the lateral boundaries in the Pi chamber experiment are not adiabatic (Chang et al. 2016; Prabhakaran et al. 2020; Shawon et al. 2021). This eliminates the mean advection contribution from Eq. (2) as the average vertical velocity is zero, and thus the equation reduces to

$$0 = -\frac{\partial}{\partial z}(\overline{F'\mathbf{w}'}) + \frac{\partial}{\partial z}(w_d\overline{F}) - \frac{\partial}{\partial r}(\overline{F}\,\overline{\dot{r}}) - \frac{\partial}{\partial r}(\overline{F'\dot{r}'}) + I\delta(r - r_i). \tag{3}$$

The growth term can be expressed in terms of saturation ratio $S = \overline{S} + s'$ as

$$\dot{r} = \underbrace{\frac{1}{r}\frac{\overline{S} - \left(1 + \frac{a}{r} - \frac{b}{r^3}\right)}{F_k + F_d}}_{\overline{\dot{r}}} + \underbrace{\frac{1}{r}\frac{s'}{F_k + F_d}}_{\dot{r}'}, \tag{4}$$

where a is the curvature coefficient, b is the solute coefficient, and F_k and F_d are the heat conduction and vapor diffusion

terms, respectively (Yau and Rogers 1996). Substituting Eq. (4) in Eq. (3), we obtain

$$\frac{\partial}{\partial z}(\overline{F'\mathbf{w}'}) - \frac{\partial}{\partial z}(w_d\overline{F}) = -\frac{\partial}{\partial r}\left[\frac{\xi\overline{F}\,(\overline{S}-B)}{r}\right] - \frac{\partial}{\partial r}\left(\frac{\xi\overline{F's'}}{r}\right) + I\delta(r-r_i), \quad (5)$$

where $B = 1 + a/r - b/r^3$ is the growth barrier, and $\xi = 1/(F_k + F_d)$ is the growth parameter (Yau and Rogers 1996). Based on the relative significance of the mean-growth term and the turbulent-growth term, three different regimes were identified in Prabhakaran et al. (2020) for the activation of cloud droplets. In regime 1, referred to as the "mean-dominant regime," the mean-growth term is dominant compared to the fluctuating growth term, i.e., $\overline{F}(\overline{S}-B) \gg \overline{F's'}$. This regime can be represented as $\overline{S} - S_c \gg \sigma_s$, where $\overline{S}$ is the mean saturation ratio, S_c is the critical saturation ratio of the aerosol and $\sigma_s = \overline{s'^2}$ is the intensity of saturation ratio fluctuations. In regime 2, referred to as the "fluctuation-influenced regime," the magnitude of the fluctuating growth term is comparable to the mean-growth term, i.e., $\overline{F}(\overline{S}-B) \sim \overline{F's'}$ and $\overline{S} > B\,\forall\, r$, i.e., $\overline{S} > S_c$. In regime 3, $\overline{S} < S_c$, referred to as the "fluctuation-dominant" regime, where activation is dominated by the fluctuating growth term. This suggests that $\overline{F's'} > 0\ \forall\ r < r_c$. Additional details on the activation regime classifications are available in Prabhakaran et al. (2020) and Shawon et al. (2021). In this study, we focus on the role played by the supersaturation fluctuations in the growth of cloud droplets in these three regimes. The key aspect is to understand the structure of $\overline{F's'}$ and its net contribution to the mean droplet size distribution in the three regimes.

3. Large-eddy simulation details

The LES results presented in this article are obtained using the System for Atmospheric Modeling (SAM) (Khairoutdinov and Randall 2003) that was configured for simulating the Pi chamber. A detailed description of the setup is provided in Thomas et al. (2019). A microphysical method of moments based on Chen and Lamb (1994) is used to simulate the microphysical processes in the Pi chamber (Yang et al. 2022). The cloud droplet size distribution is represented by a few tens of fixed bins. In each bin, cloud droplet number concentration and mass concentration are the two prognostic variables. The domain size used in this study is 1 m in the vertical and 2 m in the horizontal, and was discretized using a uniform grid size $64 \times 64 \times 32$ of 0.031 25 m. We ran another simulation with a higher-resolution and the results are consistent with the simulations presented here. See appendix for details and a brief discussion about the resolution in this study. The turbulent convection is sustained through an unstable temperature difference of 14 K across the saturated top and bottom plates. We use adiabatic conditions at the sidewalls for temperature and water vapor mixing ratio. Please note that the sidewalls are not adiabatic in the experiments (Chang et al. 2016). All the boundaries have no-slip and no-penetration boundary conditions for velocity. A monodisperse sodium chloride aerosol of size 125 nm in diameter is injected into the chamber uniformly at a constant rate. Cloud droplet activation is parameterized based on Köhler theory. All dry aerosols are activated as cloud droplets in relatively clean conditions, if the environmental supersaturation is larger than its critical supersaturation. Partial activation is considered in polluted conditions (Yang et al. 2022). Specifically, if the activation of all aerosols leads to a subsaturation, only 20% of the dry aerosol is activated as cloud droplets such that the supersaturation is still positive after activation. Newly activated cloud droplets are added in the first cloud microphysical bin. We use 33 bins to represent the cloud droplet size distribution. The bin boundaries are at doubling-mass locations starting from 1 μm (i.e., the left boundary of the first bin for cloud droplets). Number concentration and mass concentration in each bin are prognostic variables. We consider the activation, condensation, and sedimentation of cloud droplets, while solute and curvature effects, regeneration of aerosol due to evaporation, and collision between cloud droplets are ignored in this study. Solute and curvature effects are important for the growth of haze particles and cloud droplets closer to its critical radius (about 0.9 μm in radius in this study) (Devenish et al. 2012). Additionally, solute effects are important for polydisperse aerosol with very large aerosol (giant nuclei). Furthermore, a proper representation of the activation process as well as solute and curvature effects needs more efforts in model development, which is out of the scope of this study. The system reaches steady state when the activation rate of aerosol is balanced by the removal rate of cloud droplets by sedimentation. The simulation was integrated for 2 h and reaches steady state in less than 30 min for all the cases. The data from the last 1 h were used for computing the statistics. Please note that including the solute and curvature effects would change the time required to reach steady state with higher injection rate cases requiring longer to attain steady state.

4. Results

In this section, we analyze the data from the large-eddy simulations (LES) using the formalism described in section 2. This allows us to determine the contributions of all the terms in shaping the DSD [Eq. (5)], and to understand the relative roles of the terms, especially the behavior of $\overline{F's'}$ in the three regimes described in section 2. We present a localized control volume analysis (i.e., at each horizontal layer) of the DSD, accounting for all the contributions from Eq. (5). In this study only the resolved components are used for calculating all the terms (see appendix for details).

Figure 1 shows the average cloud droplet size distribution (DSD) $\overline{F}$ at three different z locations (≈0.375 m, 0.5 m, 0.625 m) for four different aerosol injection rates (Table 1). These four cases are labeled as A, B, C, and D. These size distributions indicate that the volume away from the boundaries is well-mixed as the variation in $\overline{F}$ across these vertical locations is weak. Furthermore, we observe that as the injection rate I is increased, the number concentration of cloud droplets increases and the mode in $\overline{F}$ shifts to a smaller size. Note that the data range in x and y axes in Fig. 1 are different for each panel. These results are consistent with the experimental

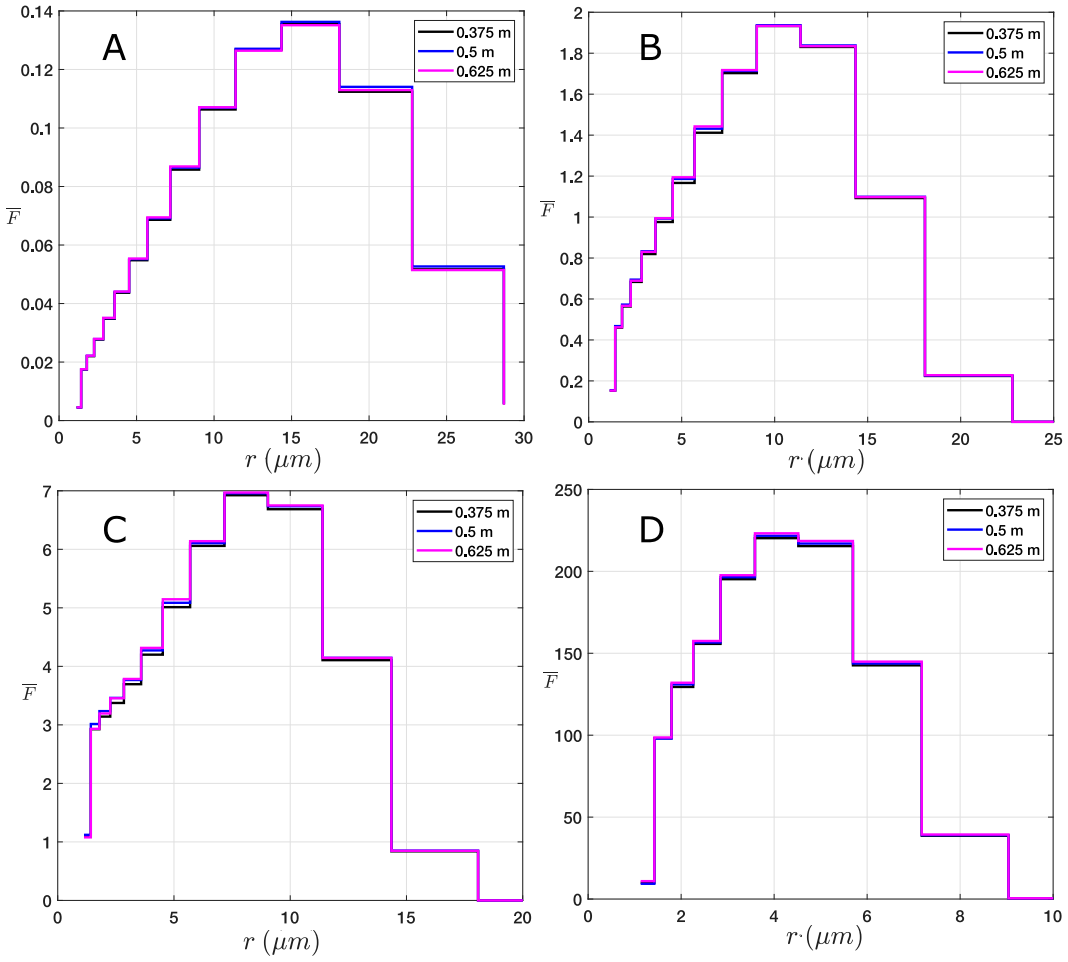

FIG. 1. Average droplet size distribution ($\overline{F}$, units: cm^{-3} μm^{-1}) for different aerosol injection rates at three different vertical locations (legend) in the chamber: (a) case A, (b) case B, (c) case C, and (d) case D. The DSD shifts toward smaller sizes from case A to D. Note that the scales for r and $\overline{F}$ differ from case to case.

observations in Chandrakar et al. (2016) and Prabhakaran et al. (2020). Since the DSDs are in a stationary state, there exists a dynamic balance between the terms in Eq. (5) where the injection rate is replaced by the net activation rate. The activated droplets grow by both mean and fluctuating saturation ratio, and this growth is balanced by the removal of droplets (turbulent transport + gravitational sedimentation) from the volume under consideration. From this dynamic balance, we determine the contributions of each of the terms in Eq. (5) for all r. The microphysical properties of all the cases investigated in this study are reported in Table 1. The radial derivatives in Eq. (5) were computed using the second-order central difference scheme.

a. *Droplet size distribution budget*

Figure 2 shows the contribution of all the terms in Eq. (5) at three different vertical locations for the cases shown in Fig. 1. In this plot, a positive (negative) contribution indicates a source

TABLE 1. Microphysical properties at the midplane ($z \approx 0.5$ m) for all the cases discussed in this article: A is mean dominant, B and C are fluctuation influenced, and D is fluctuation dominant. The saturation ratio reported here is obtained after the system reaches a steady-state post aerosol injection. $\overline{D}$ is the mean radius of the DSD, σ_D is the standard deviation of the DSD, N_d is the number concentration of the droplets, and LWC is the liquid water content.

Case ID	$\overline{S} - 1$ (%)	Aerosol injection rate (cm^{-3} s^{-1})	$\overline{r}$ (μm)	σ_D (μm)	N_d (cm^{-3})	LWC (g kg^{-1})
A	4.8	0.008 51	10.5	6	2.2	0.03
B	0.97	0.001 702	7.1	4	22	0.1
C	0.33	0.017 02	5.6	3.2	64.6	0.14
D	0.008	0.170 19	3.5	1.5	987.0	0.32

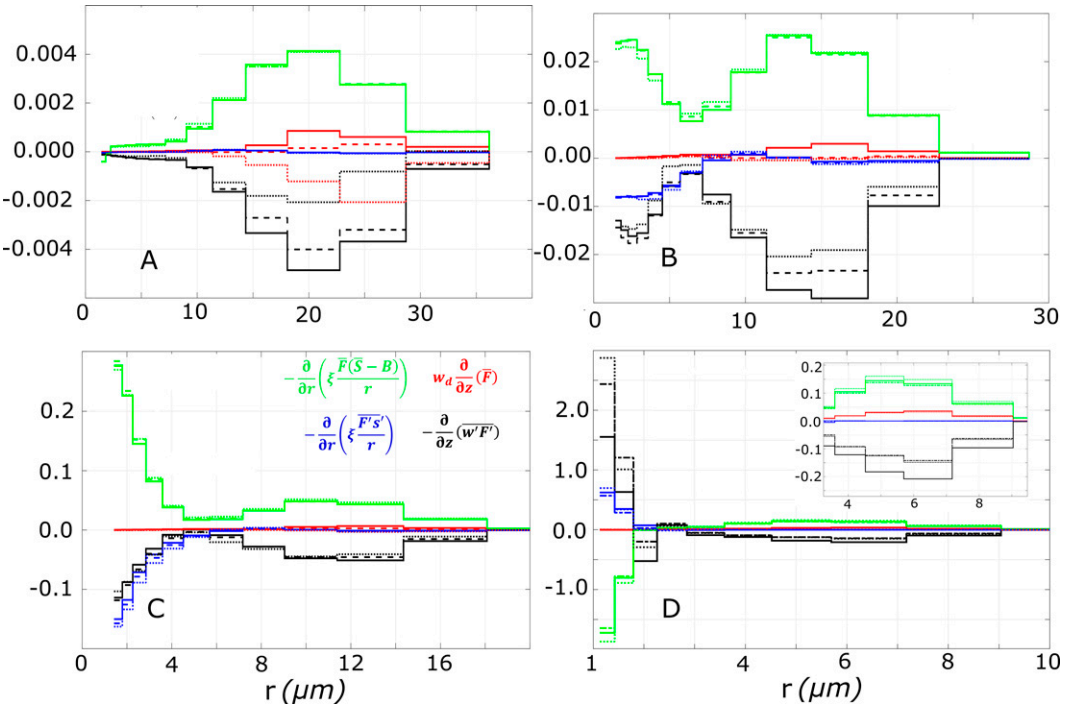

FIG. 2. Contribution of various terms to $\partial\overline{F}/\partial t$ in Eq. (5) (ordinate) for the cases shown in Fig. 1 at three different vertical locations: (a) case A, (b) case B, (c) case C, and (d) case D. Vertical location z: solid line is 0.375 m, dashed line is 0.5 m, and dotted line is 0.625 m. The inset in (d) magnifies the region in the size range of 3–9 μm. See legend in (c) for the definition of each color.

(sink) term, i.e., this term increases (decreases) the number concentration of droplets of size r. The mean-growth contribution is a dominant source term in all the cases. The contributions of the fluctuating-growth term appear to be important only in the small droplet size range. The dominant sink term in all the cases is the turbulent transport of cloud droplets from the volume (grid cell) under analysis. In the lowest injection rate case, when the droplets are sufficiently large, gravitational sedimentation effects also play an important role in droplet removal. In all cases, the net sedimentation (turbulent transport + gravitational sedimentation), is the dominant sink term in the large droplet size range. In the small droplet size range, the fluctuating-growth term also plays an important role as a sink in all the cases except cases A and D. In A this term is insignificant and in D it is an important source term. Note that the data in the first "radius" bin are strongly affected by the activation parameterization (as discussed in section 3), and thus is not shown in Fig. 2.

From Fig. 2, based on the relative significance of the mean-growth term and the fluctuating-growth term, we classify the four cases into the three regimes discussed in section 2. In case A, the contribution from the fluctuating-growth term is negligible compared to the mean-growth term at all sizes. Thus, we categorize this case to be in the "mean-dominant" growth regime. In this regime, $\overline{F}$ increases linearly with r until the sedimentation effects start playing an important role (Prabhakaran et al. 2020). The linear increase in $\overline{F}$ is evident in Fig. 1a. Since the mean-growth term is proportional to the gradient in the radius space of $\overline{F}/r$, its contribution in Fig. 2a has a very low value (near zero) until about 8–10 μm in radius after which the size dependent sedimentation effects become important. This renders the size distribution a nonlinear profile in r. In cases B and C in Figs. 2b and 2c, the fluctuating-growth term is important in the dynamic balance equation [Eq. (5)] and its magnitude is comparable to the mean-growth term, but only in the size range of small droplets. Therefore, we categorize these cases to be in the "fluctuation-influenced" regime. It is interesting to note that the mean-growth and the fluctuating-growth terms have opposing contributions in this regime. We explore this observation in greater detail later. In case D, the fluctuating-growth term is the source in the small size range and the mean-growth term is the sink, in sharp contrast to the "fluctuation-influenced" regime. This suggests that in case D the source term for the small droplets are the turbulent fluctuations in the saturation ratio, which is confirmed by the fact that $\overline{S} \approx S_c$. Based on these results, we classify case D as the "fluctuation-dominant" regime. Furthermore, in this case, the small droplets have an additional source contribution from the turbulent transport term. More details on this will be presented in the latter half of this section when we discuss the vertical variation in the saturation ratio.

b. *Covariance of F' and s'*

$\overline{F's'}$ represents the transport of cloud droplets in radius space due to fluctuations in F' and s', and s' is proportional to the variability in the condensation rate ($\dot{r}'$) due to turbulence, which is a measure of velocity in radius space. Thus, $\overline{F's'}$ is

analogous to the Reynolds stress term (momentum or heat transport) in a turbulent boundary layer. Figure 3 shows the variation of $\overline{F's'}$ as a function of r for all the cases discussed so far. In Fig. 3a, we see that $\overline{F's'} < 0$ for all the cases (A, B, and C) in the mean-dominant and fluctuation-influenced regimes (note the negative logarithmic scale). In the mean-dominant regime, the magnitude of $\overline{F's'}$ is very low and thus insignificant in shaping the average droplet size distribution. For the cases in the fluctuation-influenced regime, there is a local minimum near 6–8 μm in the shape of $|\overline{F's'}|$. The location of this minimum in the radius space is referred to as r_m. The location of r_m varies from case B to C. This is due to the decrease in mean supersaturation from case B to case C and the corresponding shift in the DSD to smaller sizes (see Fig. 1). Figure 3b shows the profile of $\overline{F's'}$ in the fluctuation-dominant regime (case D). In the small droplet size range ($r < 25$ μm), $\overline{F's'} > 0$. This observation supports the earlier conclusion that in this regime local activation occurs only due to the positive fluctuations in saturation ratio as $\overline{S} < S_c$. Additionally, in this regime, we note that the characteristic behavior of $\overline{F's'}$ varies in the vertical direction.

Figure 3 exhibits interesting features across the three regimes. In the mean-dominant regime, there is only one mode in the profile of $|\overline{F's'}|$. A similar peak in $\overline{F's'}$ is evident in the other two regimes as well (Fig. 3) for all $r \gg r_c$. The location of this mode is off from the mode in the DSD. But the peak in the magnitude of $\overline{F's'}/r$ is closer to the peak in the DSD (see Fig. 4). Furthermore, in these two regimes, the magnitude of $\overline{F's'}$ increases as r approaches the critical radius. The discussion so far suggests that there are two separate contributions to $\overline{F's'} \equiv G_s + G_l$: G_s is dominant in the small droplet size range and decreases rapidly with r, and G_l plays a significant role in the large droplet size range. In the fluctuation-influenced regime, the local minimum in the magnitude of $\overline{F's'}$ can be interpreted as the location where the importance of G_s is decreasing and G_l is increasing with r. A schematic of these two contributions to $\overline{F's'}$ is provided in Fig. 3c. A similar picture is applicable in the fluctuation-dominant regime for $\overline{F's'}$, but with its sign flipped. In all the cases, the peak in the magnitude of $\overline{F's'}$ near the large end of the DSD is due to G_l and appears to be sensitive to the mean saturation ratio. The contribution from G_l to the DSD in all the cases in this study is quite weak. Thus, a physical interpretation of G_l is not possible at the moment. Future studies including the effects of sidewalls or entrainment in atmospheric clouds may aid in understanding the behavior of G_l. Thus, additional analysis is required to ascertain the relationship between $\overline{F's'}$, the mean DSD and other parameters, and is beyond the scope of the current study. The behavior of G_s, that is dominant in the small droplet size range was discussed extensively in Prabhakaran et al. (2020). This component plays an important role in the activation of aerosol in a turbulent environment and in the growth of small droplets, but does not directly affect the large droplets significantly. The results presented in this subsection are consistent with the conclusions in the theoretical analysis presented in Prabhakaran et al. (2020) regarding the three regimes of aerosol activation and small droplet growth.

To physically interpret the quantity $\overline{F's'}$, we look at the joint frequency distribution (JFD) of F' and s' near the midplane of the simulation volume. Figure 5 depicts the JFD of F' and s' at the fourth radius bin (between 2.0 and 2.5 μm) and the tenth bin (between 8.0 and 10.1 μm) in case B (Figs. 5a,b) and at the second radius bin (between 1.3 and 1.6 μm) in case D (Fig. 5c). Note that Fig. 5 does not include the data from case A as the turbulent fluctuations are insignificant in the mean-dominant regime (see Fig. 2a). In the absence of sedimentation effects, the net flux of droplets in the radius space $\overline{F}\,\overline{\dot{r}} + \overline{F'\dot{r}'}$, is constant under steady-state conditions (Prabhakaran et al. 2020; McGraw and Liu 2006). The positive flux transports the droplets to larger diameters and the negative flux transports the droplets to smaller diameters. In Fig. 5 the contributions from the first and third quadrants are positive, and from the second and fourth quadrants are negative. The net fractional contribution (rounded off to a whole number) to the mean value of $\overline{F's'}$ from each quadrant is marked in the figure.

In the fluctuation-influenced regime, the JFD of F' and s' is aligned along the second and fourth quadrant in the small (e.g., bin 4 as shown in Fig. 5a) and big droplet (e.g., bin 10 as shown in Fig. 5b) size range. For the droplets in the large end of the distribution (bin 10), the scatterplot extends to the first quadrant as well, a point to be considered in future studies. In Fig. 5a, the dominant contributions are from the second and fourth quadrants and are nearly equal in magnitude, i.e., the positive (negative) fluctuations in the saturation ratio are correlated with the negative (positive) fluctuations in the size distribution. This suggests that the population of droplets with lower (higher) number concentration, compared to the mean concentration, grows at a faster (slower) rate in the small droplet size range due to a higher (lower) supersaturation in a local region. Thus, there is a net flux of droplets to smaller sizes as positive fluctuation in F' is correlated with the negative fluctuation in s', which explains the opposing behavior of the mean-growth term and the turbulent-growth term in this regime in Fig. 2. This would increase the number concentration of small droplets and thus would cause the small droplet tail of the distribution to broaden. Similarly, in the large end of the DSD (Fig. 5b), the dominant contribution also comes from the second and fourth quadrants. In contrast to the small end of the spectrum this would narrow the large droplet tail of the DSD as the net flux is toward smaller droplets. This differential behavior in the small (left tail) and large (right tail) end of the DSD is related to the slope of the DSD. When the slope is positive a negative flux makes the distribution broader and when the slope is negative a positive flux makes the distribution broader, and vice versa. However, the effect of the covariance term is negligible in the large droplet size range as was evident from the discussion about Fig. 2b. This is due to the size dependent removal of cloud droplets (see section 4c for details) and the factor $1/r$ in Eq. (5). The effect of the turbulent growth term diminishes by a factor of 4 from bin 4 to bin 10 in this case. This indicates that the supersaturation fluctuations are not directly effective in the flux of droplets at large droplet sizes, in contrast to the small droplets in the fluctuation-influenced regime.

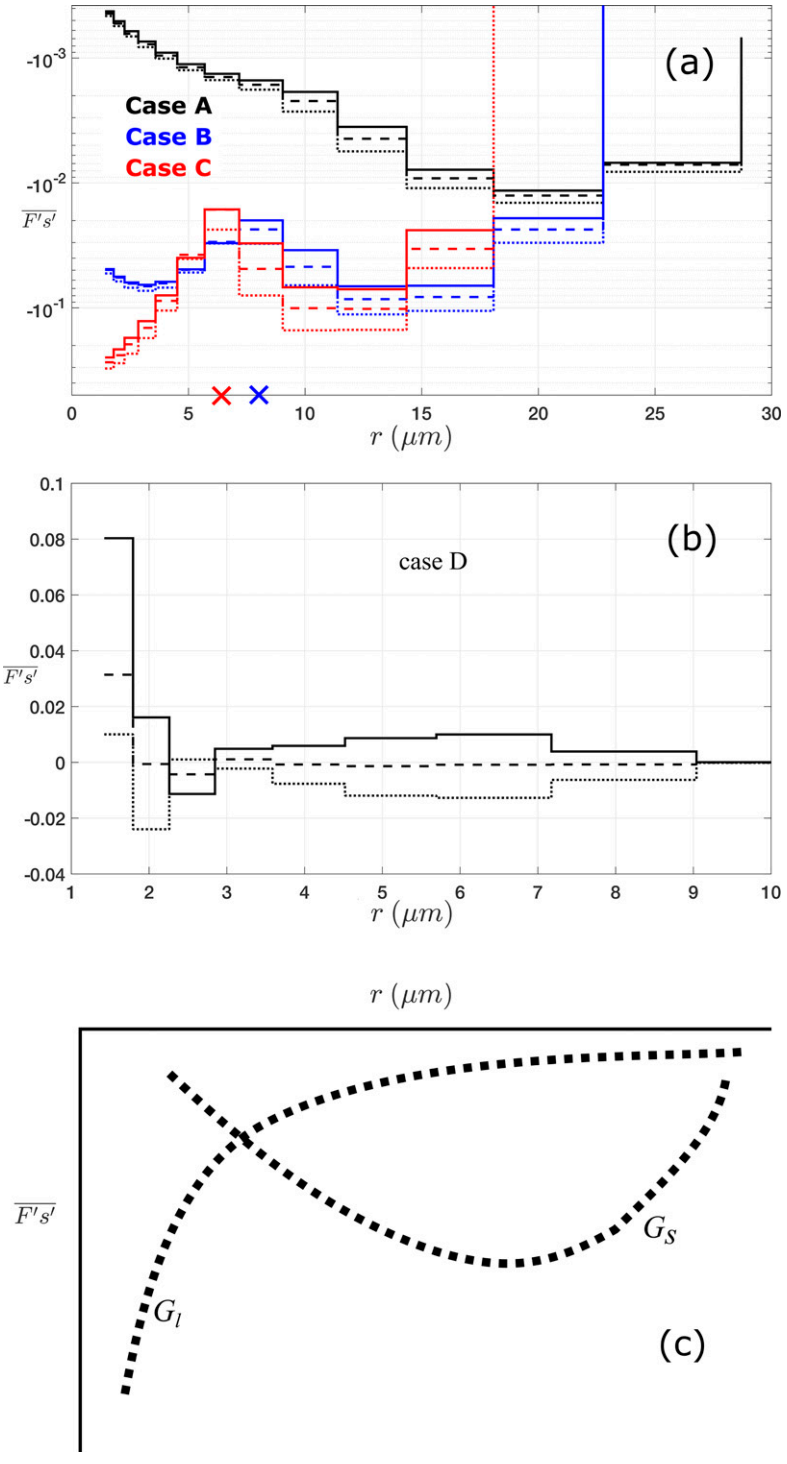

FIG. 3. Variation of $\overline{F's'}$ for the cases shown in Fig. 1 at three different vertical locations. (a) Cases A–C (note the negative logarithm on the y axis). The colored cross mark on the x axis marks the location of r_m for cases B and C. (b) Case D. Vertical location: solid line is 0.375 m, dashed line is 0.5 m, and dotted line is 0.625 m. (c) A schematic of the two contributions to $\overline{F's'} \equiv G_s + G_l$ in the fluctuation-influenced regime. Marked in the figure are the individual contributions of G_l and G_s. The sign of $\overline{F's'}$ changes from negative in cases A–C to positive (partly) in case D.

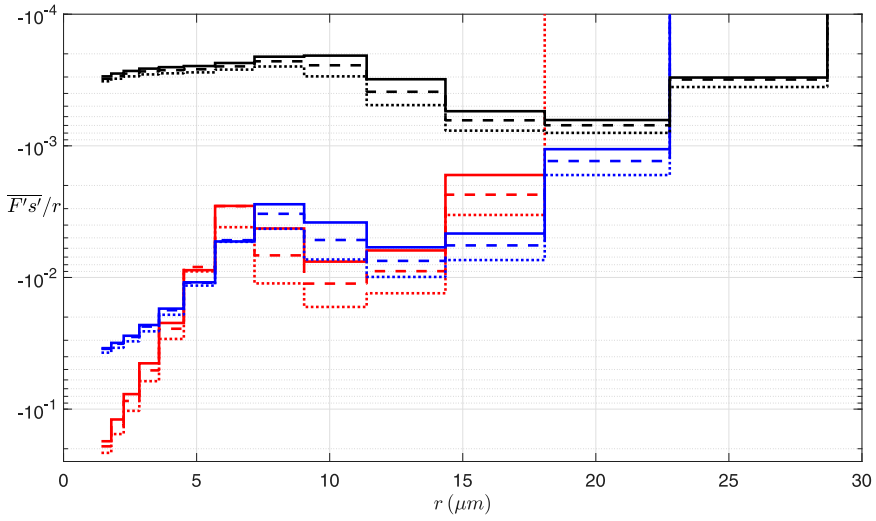

FIG. 4. $\overline{F's'}/r$ vs r in cases A, B, and C. See Fig. 3 for the color code.

Figure 5c shows the JFD for case D (fluctuation-dominant regime) in bin 2 ($r \approx 1.8\ \mu$m). This JFD is spread across all four quadrants with a slight tilt favoring quadrants 1 and 3. This would explain the positive value of $\overline{F's'}$ for this bin in Fig. 3b. The dominant contribution is from the first quadrant and is greater than the mean value, followed by the third quadrant. Additionally, there were also significant contributions from the second and fourth quadrants which were cancelled by the contributions from the third quadrant and the excess contribution from the first. Since the contributions from the first quadrant is in excess of the mean value it is enough to understand the behavior in the first quadrant to model $\overline{F's'}$. This suggests that in this regime the positive fluctuations in number concentrations are often correlated with the positive fluctuations in supersaturation in the small end of the DSD. Thus, supersaturation fluctuations play an important role in the activation and growth of cloud droplets in this size range. This behavior is very different from what we had observed in the fluctuation-influenced regime.

In a cloudy environment, in the absence of vertical velocity fluctuations, the production of supersaturation fluctuations is directly linked to the variability in the number concentration and turbulent mixing (Cooper 1989; Korolev and Mazin 2003). Thus, it is essential to understand how s' is correlated with N' in these simulations. Figure 6 shows the JFD of s' and N' in cases B and D, where $N' = \int_0^\infty F' dr$.. The structure of N' and s' covariance is qualitatively similar to those of F' and s'.

c. Droplet removal

In this subsection, we discuss the removal of cloud droplets in the current Pi chamber simulations. As was stated earlier, the transport of cloud droplets plays an important role in the evolution of the mean DSD. It is the dominant sink term in cases A and B, and is significant in cases C and D. In case A (mean-dominant regime), as shown in Fig. 2, the turbulent transport term has a single mode. But in the fluctuation-influenced regime (cases B and C), the magnitude of the turbulent transport term has a minimum [see Fig. 2 (cases B and C)] in the radius space. The location of the minimum in the magnitude of the shape of the turbulent-transport term is such that above this size the effect of the fluctuating-growth term is negligible. Note the negative value of the turbulent-transport term. This indicates that the increased turbulent transport in smaller sizes is related to the effects of turbulent fluctuations in the saturation ratio. This is evident from the variance of the size distribution fluctuation defined as $\overline{F'^2}$ in case C as shown in Fig. 7. The enhanced intensity in smaller sizes appears to be related to the effect of supersaturation variability as was discussed in sections 4a and 4b. A more detailed analysis including the explicit treatment of haze droplets is required to assess this and will be discussed separately. In case D, the turbulent transport is an important source term in the small droplet size range. This is due to the increase in saturation ratio close to the top and bottom boundaries as shown in Fig. 8 [see Chandrakar et al. (2020a) for additional details]. The mean saturation ratio in cases B, C and D is nearly uniform in the bulk and strong variation is evident close to the boundaries. This effect is significant in case D as the mean saturation ratio is supercritical ($\overline{S} > S_c$) only close to the boundaries. As a consequence, a significant fraction of the aerosol that activate near the boundaries are transported toward the midplane. This explains why the turbulent transport term is a source term along with the saturation ratio fluctuations in the small droplet size range for case D (see Fig. 2d).

In Eq. (5), the net sedimentation terms on the left side are balanced by the injection and growth terms on the right-hand side. In a steady, homogeneous system, the terms on the right-hand side of Eq. (5) are a constant. In cases A, B, and C, the sum of turbulent transport contributions and droplet sedimentation terms in Eq. (5) appear to be independent of the vertical location near the midplane (far away from the boundaries). This suggests that the net droplet flux varies linearly

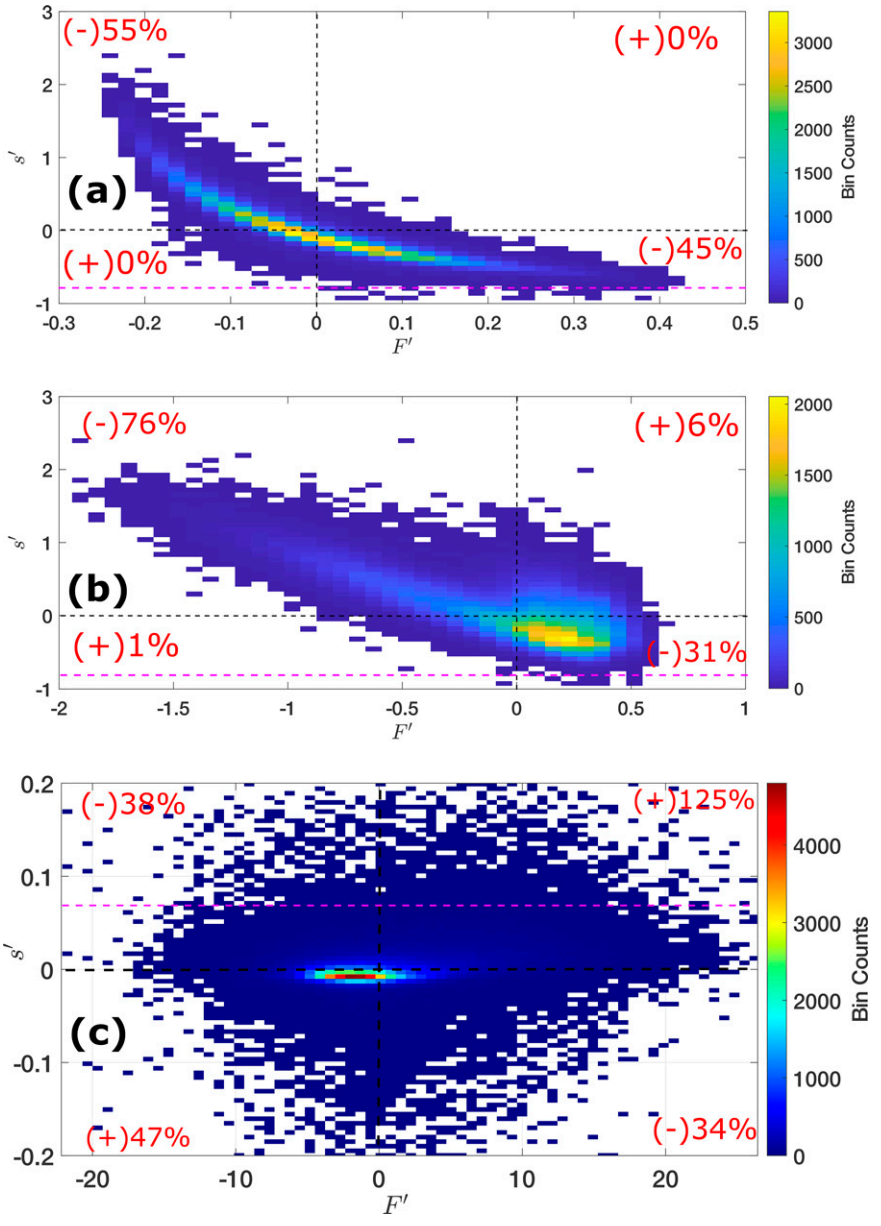

FIG. 5. Joint frequency distribution of F' ($\mathrm{cm}^{-3}\ \mu\mathrm{m}^{-1}$) and s' for cases in the fluctuation-influenced and fluctuation-dominant regimes near the midplane. The first quadrant is represented by F' and $s' \geq 0$. The second, third, and fourth quadrants are sequentially identified in the counter clockwise direction from the first. (a) Case B, fourth radius bin. (b) Case B, tenth radius bin. (c) Case D, second radius bin. The magenta line represents $S_c - \overline{S}$. The contribution from each quadrant toward $\overline{F's'}$ is mentioned in red and rounded off to the nearest integer. Note that the contributions from quadrants 2 and 4 are negative.

with height, i.e., $\overline{w'F'} - w_d\overline{F} \sim z$. Since, the size distribution is nearly homogeneous (to the leading order) in the bulk, the net turbulent droplet flux varies linearly with height for all sizes. Near the boundaries this would not be applicable due to the spatial variability introduced by the boundaries. This would alter the mean saturation ratio and the turbulence intensity near the boundaries compared to the bulk. Additionally, the effects of the boundaries are not resolved in this study. Thus, in the current system, the sedimentation effects in the bulk would adjust to the net sedimentation values near the boundaries. For the purpose of this study, it is sufficient to know the net sedimentation flux and its variation as a function of r in the homogeneous bulk region.

Figure 9 shows the vertical profile of the droplet flux for cases B and D in the small and the large droplet size range. In all cases we note that the profile of the flux is nearly linear in

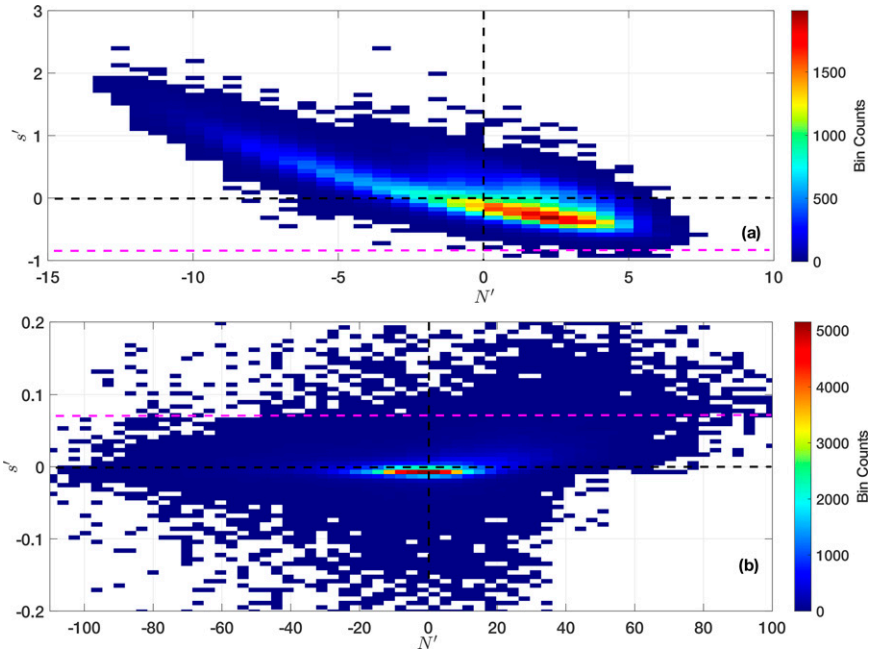

FIG. 6. Joint frequency distribution of N' (cm^{-3}) ($= \int_0^\infty F' dr$, i.e., integrated over the full size distribution) and s' for cases in the fluctuation-influenced and the fluctuation-dominant regimes: (a) case B and (b) case D. The magenta line represents the critical saturation ratio.

the bulk as was discussed above. The slope is positive in almost all cases except in the small droplet size range in case D. A positive slope in $\overline{w'F'}$ indicates a net flux of droplets toward the bottom boundary (in the direction of gravity). In the small droplet size range in case D, the negative slope in the bulk indicates a net transport of particles from the bottom boundary to the bulk. This is consistent with the observations in Fig. 2d where the turbulent transport term is the dominant source term in the size range of the small droplets. Furthermore, away from the bulk (i.e., near the top and bottom boundaries), the vertical profile of $\overline{w'F'}$ is strongly nonlinear and could be related to the enhanced mean saturation ratio and its intensity near the boundaries [Chandrakar et al. (2020a)].

It is important to know that in the DSD budget equation [Eq. (5)] the absolute value of the flux is important near the boundaries. Away from the boundaries (in the well-mixed region), it is the gradient of the flux that is important. The analysis presented so far suggests that the removal of droplets in the Pi chamber is dominated by the turbulent transport. There appears to be two modes contributing to the net transport of the droplets: one dominant in the small size range and another dominant in the large droplet size range. Thus, a Stokes sedimentation flux-based models (Krueger 2020;

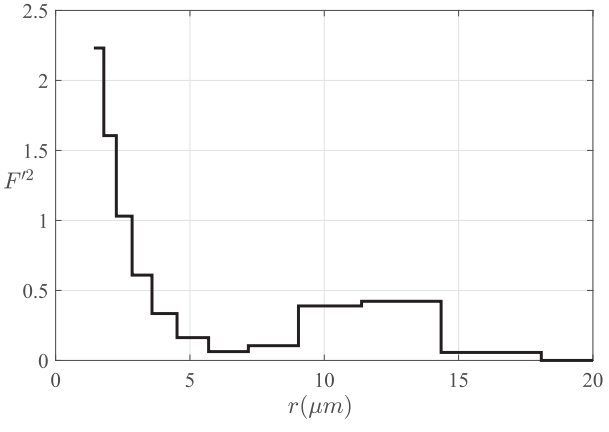

FIG. 7. Variance of the size distribution fluctuation in the midplane ($z = 0.5$ m) as a function of r in the fluctuation-influenced regime (case C). Note the local minimum at radius of 6–8 μm.

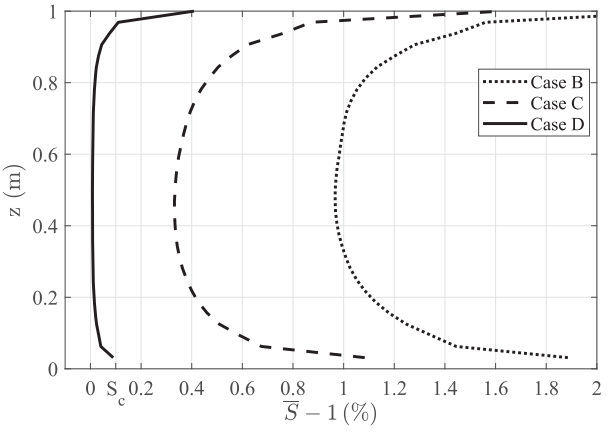

FIG. 8. Vertical variation of $\overline{S}$ in cases B, C, and D. On the x axis, S_c represents the critical saturation ratio of the aerosol.

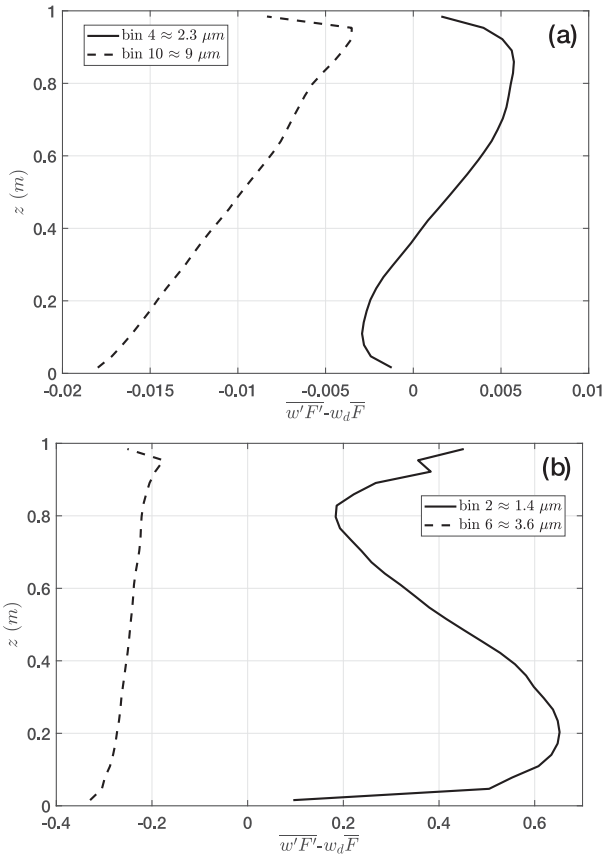

FIG. 9. Droplet flux (turbulent transport and gravitational sedimentation flux) in cases B and D. (a) Case B, fourth and tenth bins. (b) Case D, second and sixth bins.

Chandrakar et al. 2020b) may not be sufficient to obtain the full DSD budget. Additional analysis is required to understand the droplet sedimentation in the Pi chamber with emphasis on the diffusive layers close to the boundaries. A direct numerical simulation study with a fully resolved boundary flow would be useful in this regard.

5. Discussion

In section 4, a comprehensive analysis of various processes that shape the DSD in the Pi chamber were analyzed from a high resolution LES dataset. The analysis revealed the significance of all the terms in Eq. (5) at different droplet size range in all the three regimes. In this section, we use the results from these simulations to discuss the existing experimental observations and theoretical models of the Pi chamber. Despite the idealized nature of the simulations, the adiabatic sidewalls aid in reducing the system into a one dimensional problem, which simplified the analysis significantly. Simulations using more realistic conditions, including the Kelvin and Raoult terms in the activation and growth of droplets, will be reported in the future. Furthermore, we use the insights from the Pi chamber studies to discuss the conclusions related to DSD broadening from the recent turbulent adiabatic cloud parcel studies.

a. Pi chamber

From the results presented in section 4, we know that in the mean-dominated and fluctuation-influenced regimes, the changes in the DSD due to aerosol forcing are dominated by the changes in the mean-saturation ratio. The supersaturation fluctuations play a significant role only in the small droplet size range in the fluctuation-influenced regime. In the fluctuation-dominant regime (case D), fluctuations play a primary role in the formation and growth of small cloud droplets, but the subsequent growth is dominated by the mean-saturation ratio. The fluctuation-dominant regime has two sub-regimes: (i) $1 < \overline{S} \leq S_c$ and (ii) $\overline{S} \leq 1$. Case D, discussed in section 4, was in sub-regime (i) of the fluctuation-dominated regime. Sub-regime (ii) is not explored in this study as it requires subsaturating at least one of the boundaries or requires a high concentration of large hygroscopic aerosol particles, and thus is beyond the scope of the current study. The discussion so far suggests that the decrease in the width of the DSD with an increase in aerosol injection rate observed in Chandrakar et al. (2016) and Prabhakaran et al. (2020) is primarily due to the reduction in the mean-saturation ratio from the increase in the droplet concentration (and integral radius) and is not due to the reduction in the intensity of saturation ratio fluctuations. In a turbulent environment, the saturation ratio is a fluctuating quantity. The concept of stochastic condensation is based on the idea that a group of cloud droplets that encounter variable and/or different growth histories would encounter different effective growth rates (Cooper 1989). This would lead to broadening of the droplet size distribution. A similar idea was used in Chandrakar et al. (2016) where the supersaturation fluctuations were modeled as a Gaussian random variable; the effects of those fluctuations on the width of the DSD were then obtained analytically. (see Sardina et al. (2015), Chandrakar et al. (2016), and Saito et al. (2019) for additional details on the stochastic condensation framework.) The key assumptions in these studies are: (i) mean supersaturation is close to zero and hence is negligible, (ii) all the droplets in the system have the same lifetime, and (iii) supersaturation is treated as a Gaussian random variable with no additional constraints.

In experiments and field campaigns, it is very challenging to measure the absolute saturation ratio accurately under cloudy conditions due to instrumentation limitations (Siebert and Shaw 2017; Anderson et al. 2021). So, in theoretical modeling studies, a value for the mean saturation ratio is often assumed (Chandrakar et al. 2020b). On the other hand, in high-resolution LES studies, like the one presented in section 4, one can obtain mean saturation ratio and its intensity to high accuracy. Thus, in theoretical studies assuming a value for the mean saturation ratio may restrict the cloud system to a specific regime. This may influence the nature of the effect of supersaturation fluctuations on the DSD and may create an inconsistency between the theory and observation. As was stated earlier, the recent studies on stochastic condensation are based on a Lagrangian framework and one of the fundamental assumptions in all these studies is that all the droplets have the same lifetime (Chandrakar et al. 2016; Sardina et al. 2015). The analysis presented in section 4 is

an Eulerian viewpoint of the cloud system in the Pi chamber. As a consequence, the lifetime of individual droplets cannot be calculated from the current analysis. Nevertheless, from the results in section 4 we know that sedimentation flux of particles is not uniform and is regime dependent. The turbulent transport of droplets appears to be the dominant removal term. In the large droplet size range there appears to be an r^2 dependence in the sedimentation flux. A similar model was also used in (Krueger 2020) for the removal of cloud droplets. These observations suggest that there is a preferential removal of large particles. Thus, in the context of the Lagrangian stochastic condensation framework, all the particles cannot have the same lifetime. The population of particles that encounter higher supersaturation grow quickly to large enough diameters after which sedimentation will dominate. On the other hand, the population of particles that encounter lower supersaturation will grow slowly but for longer duration until sedimentation effects become important. So, what matters is the integrated effect of supersaturation over the life time of droplets and thus the Lagrangian framework needs to be modified to account for the differences in the lifetime of different droplets. A similar conclusion was obtained from a recent DNS study of the Pi chamber (MacMillan et al. 2022).

To account for the size dependent sedimentation effects in the stochastic condensation framework, Chandrakar et al. (2020b) explored the shapes of DSD using a Fokker–Planck model based on the Langevin equation. This is equivalent to Prandtl's mixing length/eddy-diffusivity based closure but in the "radius" space instead of physical space. (See Khvorostyanov and Curry 1999; Manton 1979 for more details.) The main point of the eddy-diffusivity model is that the covariance between supersaturation fluctuations and size distribution fluctuations are represented as the diffusive transport of mean size distribution $\overline{F}$ in the "radius" space, i.e., $\overline{F'\dot{r}'} \equiv \xi(\overline{F's'}/r) = -D(d/dr)\overline{F}$, where D is the turbulent diffusivity in "radius" space. In all the cases considered here $\overline{F}$ has a peak. This would suggest that the modeled $\overline{F's'}$ will be negative to the left of the peak and positive after the peak. This modeled behavior of $\overline{F's'}$ is inconsistent with the results presented in section 4 (see Fig. 3). In the mean-dominant and fluctuation-influenced regimes, $\overline{F's'} < 0 \; \forall \; r$. For the case in the fluctuation-dominant regime, $\overline{F's'}$ approaches a value of zero around $2 < r < 3$ μm, but it does not coincide with the location of the peak in the size distribution. Thus, the modeled shape of $\overline{F's'}$ using the mixing-length approach appears to be inconsistent with the results reported in section 4. In Chandrakar et al. (2020b), the Fokker–Planck model was used in the r^2 space. In the r^2 space, the turbulent closure term is $f'\dot{r^2}'$ where $f(r^2) = F(r)/2r$. The mixing-length closure for this is $f'\dot{r^2}' = -D^*(d/dr)\overline{f}$, where D^* is the turbulent diffusivity in the r^2 space (Manton 1979). The resulting equation is the drift-diffusion equation obtained from the Fokker–Planck framework (Chandrakar et al. 2020b). The mixing-length based closure is similar in r and r^2 space. Thus, the issues raised earlier regarding the closure in the r space is applicable to the closure in the r^2 space. Similar limitations of the constant eddy-diffusivity models (also known as mixing-length or gradient transport models) are well known in other conventional turbulent flows, e.g., convective boundary layers (Deardorff 1966) or turbulent wall jets (Narasimha 1990). Thus, a more nuanced treatment of turbulent closure schemes is required in cloud microphysics as well. For instance, it might be worthwhile to consider different schemes for each regime. Additionally, the eddy diffusivity models may still be applicable in the fluctuation-dominated regime (b) (where $\overline{S} \leq 1$) which is not explored in this study.

An additional key assumption used in the stochastic condensation model based on a Lagrangian framework is that the saturation ratio fluctuation is a random Gaussian variable (Chandrakar et al. 2016; Saito et al. 2019; Chandrakar et al. 2020b). A recent study based on a Gaussian mixing model has shown that the saturation ratio distribution obtained from mixing processes could have non-Gaussian effects [Thomas et al. (2021)]. Furthermore, the insights presented in Fig. 5 and the related discussions in section 4 indicate that the saturation ratio fluctuations have a structure (i.e., shape of the F' and s' scatterplot that determines $\overline{F's'}$) and are not an unconstrained random variable. The structure of the covariance between F' and s' varies in all three regimes and this information needs to be encoded into any saturation ratio forcing used in the stochastic Lagrangian formulation. This covariance is affected by the mean saturation ratio, lifetime of cloud droplets, and the nature of the underlying turbulent flow. An incorrect representation of these quantities may lead to inconsistent results and conclusions.

At this juncture it is important to note that in the experiments reported in Chandrakar et al. (2016) and Prabhakaran et al. (2020) the sidewall conditions were not adiabatic for temperature and water vapor, unlike the current simulations. The non-adiabatic sidewalls may change the intensity of the supersaturation fluctuations and the structure of the covariance between F' and s'. Nevertheless, given the preferential removal of the large droplets and the $1/r$ factor in the covariance term, it remains to be seen how significant the effects from the sidewalls are in shaping the DSD in the Pi chamber. A full DNS study capturing activation and sidewall effects would aid in better understanding of the unresolved processes in the Pi chamber.

b. *Atmospheric implications*

In section 5a, we discussed the role of supersaturation fluctuations in the Pi chamber. Our analysis in the context of the Pi chamber showed that in the Eulerian (Lagrangian) framework, removal or transport (life time) of particles in the control volume (localized domain–e.g., horizontal slab) under consideration is an important contribution when assessing the significance of supersaturation fluctuations. In the context of atmospheric clouds, the transport of cloud droplets is a complex three-dimensional problem unlike in the Pi chamber where we have to only focus on the vertical transport. Additionally, the cloud systems are evolving in time which adds more complexity to the problem. In this subsection, we discuss the results from section 4 in the context of atmospheric clouds and also discuss how this framework can be extended to high resolution simulations of atmospheric clouds. Turbulent transport (or Lagrangian dispersion) is an important quantity in all

real world turbulent flows. In cloud microphysics, the transport of cloud droplets is related to turbulent entrainment/mixing processes and gravitational settling. The latter process is strongly size dependent. Several studies in the last several decades have discussed the role of entrainment and mixing in broadening the cloud DSD (Manton 1979; Baker et al. 1980; Telford and Chai 1980; Cooper 1989; Lasher-Trapp et al. 2005). Entrainment and mixing events introduce strong variability in the size distribution and supersaturation. These events produce a mechanism for supersaturation variability that is decoupled from the vertical velocity fluctuations, the significance of which is addressed later in this subsection. Furthermore, these processes are associated with spatial inhomogeneity that occurs at scales ranging from the cloud scale to the Kolmogorov length scale (Turner 1986). In the framework of the stochastic condensation model, the presence of spatial inhomogeneties directly leads to a group of cloud droplets encountering differential growth histories, thus resulting in a broad cloud DSD. This was shown explicitly by tracking individual cloud parcels from detailed simulations of a cumulus congestus in Lasher-Trapp et al. (2005) and Cooper et al. (2013). The cloud parcels that rise along the cloud core are relatively unaffected by entrainment. On the other hand, the parcels along the cloud edges encounter entrainment events resulting in partial evaporation of cloud droplets. This results in the formation of large cloud droplets (Yang et al. 2016). Additionally, entrained or deactivated aerosol result in activation away from the cloud base that aid in forming small droplets (Hoffmann et al. 2015). Thus, an ensemble of cloud parcels with varied growth histories result in broad DSDs which leads to the onset of precipitation in warm cumulus clouds (Cooper et al. 2013). Similar analyses were also conducted in stratocumulus clouds where it was concluded that large droplets were observed in cloud parcels that were affected by cloud-top entrainment (Kogan 2006; Wang et al. 2009; Magaritz-Ronen et al. 2014; Pinsky et al. 2016). In a nutshell, turbulent transport is an integral part of the stochastic condensation framework in atmospheric clouds, which was also evident from the Pi chamber results in section 4.

On the other hand, recent cloud parcel studies have shown that turbulent fluctuations play an important role in broadening the cloud DSD (Grabowski and Abade 2017; Sardina et al. 2018; Abade et al. 2018). Grabowski and Abade (2017) referred to this stochastic condensation framework (adiabatic turbulent parcel, i.e., no turbulent transport) as "eddy-hopping." These studies considered an adiabatic turbulent cloud parcel with constant updraft ($\overline{W}$). In such a scenario, Eq. (2) can be rewritten as

$$\frac{\overline{D}}{\overline{D}t}(\overline{F}) = -\boldsymbol{\nabla}\cdot(\overline{F'\mathbf{u}'}) + \frac{\partial}{\partial z}(w_d\overline{F}) - \frac{\partial}{\partial r}(\overline{F}\,\overline{\dot{r}}) - \frac{\partial}{\partial r}(\overline{F'\dot{r}'}) + I\delta(r - r_i, \mathbf{x} - \mathbf{x}_i), \tag{6}$$

where $\overline{D}/\overline{D}t = \partial/\partial t + \overline{W}\partial/\partial z$. In the reference frame of a cloud parcel moving with a velocity $\overline{W}$, we can express $\overline{D}/\overline{D}t \equiv \partial/\partial t$. With this simplification the interpretation of all the terms in Eq. (6) are the same as that in the context of the Pi chamber [see Eq. (2)]. In cloud parcel studies, the standard assumption is that the parcel is homogeneous and isotropic (Sardina et al. 2015, 2018; Abade et al. 2018; Saito et al. 2019). Consequently, the turbulent transport and sedimentation flux divergence terms are equated to zero, and only the growth terms are retained on the right-hand side of Eq. (6). Thus, the particles that are removed from one side of the parcel are transported into the parcel from the other side. Therefore, all the droplets in the parcel have the same life time and no net transport. Here, we discuss the limitations of these assumptions in the context of cloud parcels.

Let us consider a hypothetical cloud volume with monodisperse aerosol and uniform water vapor mixing ratio. We assume that the volume is horizontally homogeneous and thus in the horizontal direction periodic boundary conditions are applicable. We let this volume evolve over time (i.e., rise up quasi-adiabatically) and allow the aerosol to activate into cloud droplets. Since we retain the vertical variation in the system, the liquid water content would increase linearly (approximately) from the bottom to the top of the parcel. As a consequence, the droplet diameters also increase with height. We now expose this cloud parcel to turbulent fluctuations and assume that the supersaturation fluctuations are directly proportional to the vertical velocity fluctuations similar to Grabowski and Abade (2017). Since the supersaturation fluctuation is correlated with the vertical velocity fluctuation, any droplet that encounters positive supersaturation fluctuation will be transported upward. Similarly, any droplet that encounters negative supersaturation fluctuation will be transported downward. Consequently, the turbulent transport represented as $\overline{w'F'}$ will have dominant contribution from large droplets at the top boundary and small droplets at the bottom boundary. This preferential transport of large and small droplets in opposite directions may not aid in broadening the DSD locally. Thus, supersaturation fluctuations due to vertical velocity fluctuations do not aid in broadening the DSD "locally," which is essential for the onset of collision-coalescence. However, the effects of turbulent transport may partly be offset by gravitational sedimentation and Damköhler number [ratio of phase relaxation and turbulence time scale (Siebert and Shaw 2017)] effects. The former effects are relevant only for large droplets, and the latter effects might be relevant under pristine conditions. Additional studies are required to assess to what extent these effects can mitigate the effects of turbulent transport, and thus aid in DSD broadening. The cloud parcel studies in Grabowski and Abade (2017) and Sardina et al. (2018) do not account for the transport of cloud droplets appropriately which is essential for a realistic representation of the microphysics. Additionally, the imposition of periodic boundary conditions in all directions inherently ensures that all the cloud droplets have the same life time. Thus, similar to the Pi chamber there is a preferential transport (net flux divergence of turbulent transport) of droplets in a cloud parcel volume which if appropriately represented may not show significant broadening due to supersaturation fluctuations related to vertical velocity variability. These arguments related to the limitations of the DSD broadening due to eddy-hopping or vertical velocity fluctuations are not new and were discussed extensively in Mazin and Smirnov (1969), Bartlett and Jonas (1972), Manton (1979), and Cooper (1989).

Recent parcel studies have tried to address these questions by treating supersaturation as a stochastic variable and solving the evolution of the cloud field using DNS within the framework of an idealized cloud parcel (Sardina et al. 2015; Siewert et al. 2017; Grabowski et al. 2022). In these studies, the cause of supersaturation fluctuations are not accounted for, and all the particles/droplets have the same life time. Limitations of these assumptions were discussed earlier in the context of the Pi chamber and cloud parcels. Furthermore, since the supersaturation fluctuations are treated as a Gaussian random variable, it may not satisfy the covariance of F' and s', such as the one shown in Fig. 5 for the Pi chamber simulations. The structure of the scatterplot adds an additional constraint on the behavior of s', which is not accounted for in these idealized studies. Thus, the existing studies of stochastic condensation based on an adiabatic cloud parcel framework are inadequate to ascertain if the fluctuations in supersaturation aid in broadening the large droplet tail of the DSD in atmospheric clouds.

The Lagrangian mixing parcel analysis shown in Lasher-Trapp et al. (2005) aids in conceptually understanding the stochastic condensation framework, but does not quantify the importance of various terms in shaping the DSD. In that context, the framework used for analyzing the Pi chamber simulations in section 4 quantify the importance of all the terms relevant in shaping the DSD. This may serve as a basis for better parameterization of the cloud microphysical properties in numerical models. A key advantage in the analysis of the Pi chamber data were that the simulation was in the stationary state and so time averaging of the dataset was possible. Atmospheric clouds are seldom in a steady state. In such a scenario, one can replace time average with ensemble average and can also exploit any symmetries in the cloud system. For instance, in closed cell stratocumulus clouds the horizontal homogeneity of the cloud systems can be used for averaging. A similar analysis was conducted in Wang et al. (2003) to budget the liquid water content in non-precipitating stratocumulus clouds and can be extended to understand the role played by turbulence in shaping the DSD in these clouds. Additionally, to separate the updraft and downdraft effects in stratocumulus clouds phase averaging could also be used. In the context of cumulus clouds, apart from ensemble averaging one could use cloud edge-based averaging to compute the required statistics. This would aid in determining the cloud properties relative to the location of the cloud edge. This is a standard procedure for studying entrainment processes in free-shear turbulent flows (e.g., jets, plumes, wakes etc.) (da Silva et al. 2014). A similar procedure was used in Nair et al. (2020) to understand the dynamics of the subsiding shells in cumulus clouds, and thus can be extended to understand the shape of the DSD in cumulus systems from high-resolution LES data. We argue that the Eulerian analysis described here would provide a proper attribution of $\overline{S}$, s', turbulent transport, and sedimentation on the shape of the DSD.

6. Summary

In this study, we established a framework for assessing the role of turbulence in cloud microphysics using high-resolution data. We explored the role played by mean supersaturation, supersaturation fluctuations, turbulent transport, and gravitational sedimentation in the growth of cloud droplets in the Pi chamber. The analysis revealed that in the Pi chamber the role of supersaturation fluctuations are directly important in the activation of aerosol and growth of small cloud droplets. However, the dominant role in the main mode of the DSD is played by the growth due to mean saturation ratio and turbulent transport. The preferential removal of large droplets from the chamber suppresses the effect of supersaturation fluctuations in the growth of the large cloud droplets. The effect of fluctuations is felt indirectly in the large droplet size range. For instance, with a fixed supersaturation forcing, the increase in the intensity of supersaturation fluctuations will increase the activation rate of aerosol (Shawon et al. 2021). This in turn will influence the mean supersaturation in the system, and thus affect the large end of the droplet spectrum. Thus, to determine the steady-state LWC in the Pi chamber, the knowledge of the mean saturation ratio is sufficient, provided we know the turbulent contribution to sedimentation flux and aerosol activation rate. Additionally, the results from this study were used to assess the significance of eddy-diffusivity based closure in the radius space for DSD evolution equation in the Pi chamber. The analysis showed that a straightforward implementation of such mixing-length models are not applicable in the context of the Pi chamber, although the effects of sidewalls remain unexplored which would be addressed in a future study. A more detailed, regime-dependent treatment is required to model the turbulent covariance terms in cloud microphysics.

The insights from the analysis of the Pi chamber data were used to assess the role played by stochastic condensation in broadening the DSD in cloud parcel studies. The significance of the variable droplet growth histories due to entrainment in Lagrangian mixing parcel analysis was interpreted in terms of turbulent transport in an Eulerian framework. However, the recent adiabatic turbulent cloud parcel studies where the supersaturation fluctuations are correlated with the vertical velocity fluctuations alone have suggested that large cloud droplets can form in the absence of spatial heterogeneity and mixing. We attribute this observation to the triple periodic boundary conditions and inadequate representation of vertical turbulent transport in the parcel.

In this study we have identified two sources of stochasticity induced by turbulence: one is supersaturation fluctuation and the other is turbulent transport. In the context of microphysics the effects of these two variables are intertwined, so a parcel approach is flawed even for the simplest of geometries like the Pi chamber. Thus, to assess the effects of supersaturation fluctuations in any cloud system it is essential to understand the mechanism by which supersaturation fluctuations are created and how this mechanism correlates with the transport of cloud droplets in the system.

Acknowledgments. This work was supported by NSF Grant AGS-1754244, Department of Energy Grants DE-SC0012704 and DE-SC0018931, and by the Office of Biological and Environmental Research in the Department of Energy, Office of Science, through the U.S. Department of Energy Contract DE-SC0012704 to Brookhaven National Laboratory. Portage and Superior high-

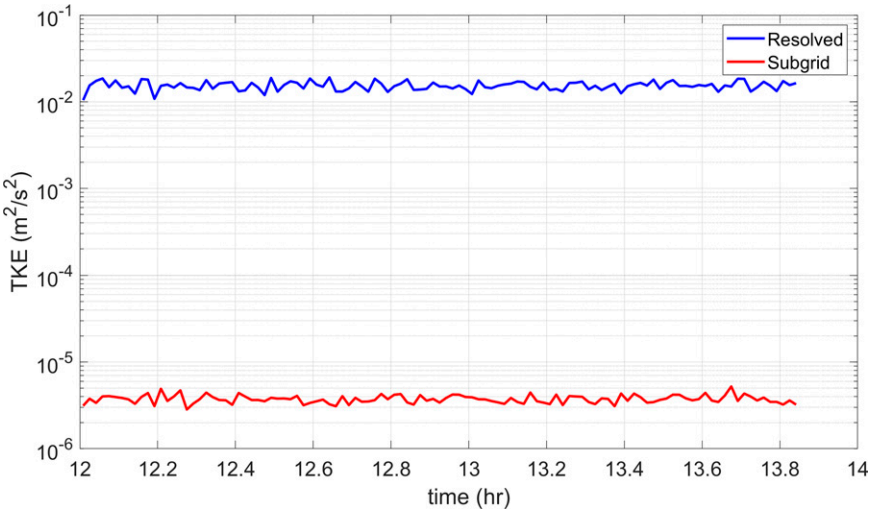

FIG. A1. Resolved and subgrid-scale turbulent kinetic energy (TKE) time series near the midplane.

performance computing infrastructures at Michigan Technological University were used in obtaining results presented in this publication.

Data availability statement. The current study used the SAM (https://wiki.harvard.edu/confluence/display/climatemodeling/SAM) for the simulations presented here. The outputs from the model used in this study are too large to be archived. The required details for simulating the cloud system are included in the main text. Additionally, the data files from the simulations will be made available upon request to the corresponding author.

APPENDIX

Significance of the Unresolved Fluxes

In this study we present the turbulent transport fluxes from the resolved part of the flow field. The flux contributions are dominated by the large-scale motions (Narasimha 1990; Pope 2000) as the unresolved small scales are homogeneous and isotropic (Kolmogorov 1941), and thus do not contribute to net transport of fluxes. The issue arises only close to the top and bottom boundaries where the interaction with the wall is not resolved. For this, a separate wall model is implemented to for the momentum, temperature, and water vapor fluxes using the Monin–Obukhov similarity parameterization. For the size distribution flux ($\overline{w'F'}$), to the best of our knowledge, a wall model does not exist. So, in the current study we only have the subgrid scale model to represent the unresolved fluxes (related to droplet transport) near the boundaries. In this article, we present the DSD budget only in the well-mixed bulk (far away from the boundaries), where the contributions from the unresolved fluxes is minimal. This is evident from the value of the subgrid scale diffusivity in the bulk region (approximately 10^{-4} m^2 s^{-1}), which is about 5–8 times the physical

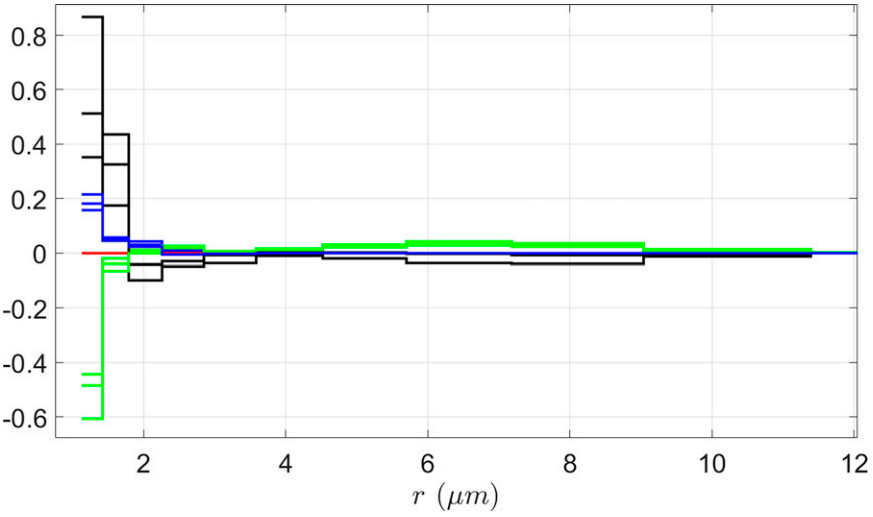

FIG. A2. DSD budget in the 2 m case analogous to Fig. 2d in the main paper.

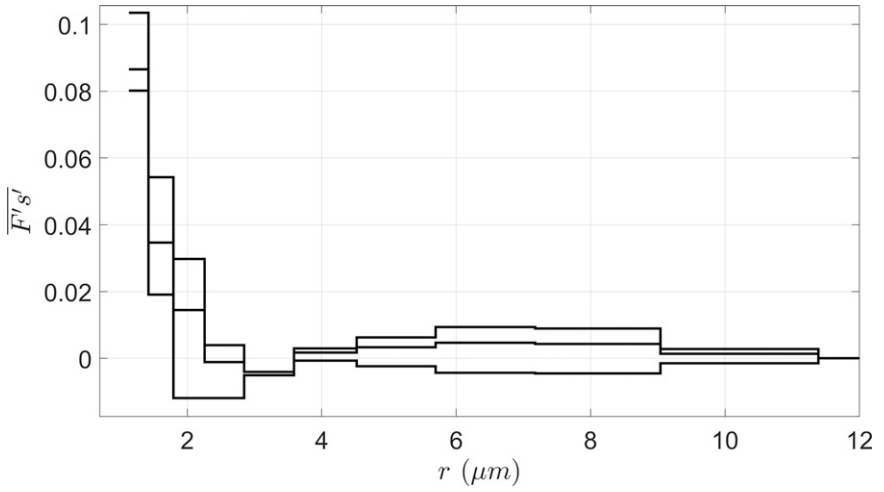

FIG. A3. $\overline{F's'}$ for the 2 m case; compare to Fig. 3b.

diffusivity in this system. This is also evident from the turbulent kinetic energy time series near the midplane shown in Fig. A1. We can see that the contributions from the subgrid scale TKE is insignificant. Thus, to convey the key message in this study the resolved components of the fluxes in the bulk is sufficient.

2 m chamber simulation

To address the issue of resolution within the framework of the current LES we ran another case where the grid size was set to 0.031 25 cm (same as in the current study), but the spatial dimensions were increased by a factor of 2 in all directions. The Rayleigh number (Ra), defined as $(g\alpha\Delta TH^3)/(\nu k)$, is a measure of turbulence intensity in a convective system. Ra in this 2 m case increases by a factor of 8 relative to the cases discussed in the main text, but the spatial resolution is the same. The largest scale increases by a factor of 2 (relative to the 1 m case), whereas the smallest scale remains the same in both cases as the mean dissipation rate is independent of height in Rayleigh Benard convection, assuming that the Nusselt number is proportional to $\mathrm{Ra}^{1/3}$ (Chillà and Schumacher 2012). Thus, in the 2-m-height case the number of resolved scales is greater than in the 1-m-height case. Figure A2 shows the DSD budget plot and the shape of $F's'$ in Fig. A3 for this case. The mean supersaturation in this case is less than S_c, which indicates that this case is in the fluctuation-dominant regime. This is also evident from the similarity between Fig. 2d and Fig. A2. Additionally, we see that the shape of $\overline{F's'}$ is similar in Fig. A3 and Fig. 3b in the main text.

REFERENCES

Abade, G. C., W. W. Grabowski, and H. Pawlowska, 2018: Broadening of cloud droplet spectra through eddy hopping: Turbulent entraining parcel simulations. *J. Atmos. Sci.*, **75**, 3365–3379, https://doi.org/10.1175/JAS-D-18-0078.1.

Albrecht, B. A., 1989: Aerosols, cloud microphysics, and fractional cloudiness. *Science*, **245**, 1227–1230, https://doi.org/10.1126/science.245.4923.1227.

Anderson, J. C., S. Thomas, P. Prabhakaran, R. A. Shaw, and W. Cantrell, 2021: Effects of the large-scale circulation on temperature and water vapor distributions in the Π chamber. *Atmos. Meas. Tech.*, **14**, 5473–5485, https://doi.org/10.5194/amt-14-5473-2021.

Baker, M. B., R. G. Corbin, and J. Latham, 1980: The influence of entrainment on the evolution of cloud droplet spectra: I. A model of inhomogeneous mixing. *Quart. J. Roy. Meteor. Soc.*, **106**, 581–598, https://doi.org/10.1002/qj.49710644914.

Bartlett, J. T., and P. R. Jonas, 1972: On the dispersion of the sizes of droplets growing by condensation in turbulent clouds. *Quart. J. Roy. Meteor. Soc.*, **98**, 150–164, https://doi.org/10.1002/qj.49709841512.

Boucher, O., and Coauthors, 2013: Clouds and aerosols. *Climate Change 2013: The Physical Science Basis*, T. F. Stocker et al., Eds., Cambridge University Press, 571–657.

Chandrakar, K. K., W. Cantrell, K. Chang, D. Ciochetto, D. Niedermeier, M. Ovchinnikov, R. A. Shaw, and F. Yang, 2016: Aerosol indirect effect from turbulence-induced broadening of cloud-droplet size distributions. *Proc. Natl. Acad. Sci. USA*, **113**, 14 243–14 248, https://doi.org/10.1073/pnas.1612686113.

——, ——, D. Ciochetto, S. Karki, G. Kinney, and R. A. Shaw, 2017: Aerosol removal and cloud collapse accelerated by supersaturation fluctuations in turbulence. *Geophys. Res. Lett.*, **44**, 4359–4367, https://doi.org/10.1002/2017GL072762.

——, ——, S. Krueger, R. A. Shaw, and S. Wunsch, 2020a: Supersaturation fluctuations in moist turbulent Rayleigh–Bénard convection: A two-scalar transport problem. *J. Fluid Mech.*, **884**, A19, https://doi.org/10.1017/jfm.2019.895.

——, I. Saito, F. Yang, W. Cantrell, T. Gotoh, and R. A. Shaw, 2020b: Droplet size distributions in turbulent clouds: Experimental evaluation of theoretical distributions. *Quart. J. Roy. Meteor. Soc.*, **146**, 483–504, https://doi.org/10.1002/qj.3692.

Chang, K., and Coauthors, 2016: A laboratory facility to study gas–aerosol–cloud interactions in a turbulent environment: The Π chamber. *Bull. Amer. Meteor. Soc.*, **97**, 2343–2358, https://doi.org/10.1175/BAMS-D-15-00203.1.

Chen, J.-P., and D. Lamb, 1994: Simulation of cloud microphysical and chemical processes using a multicomponent framework. Part I: Description of the microphysical model. *J. Atmos. Sci.*,

51, 2613–2630, https://doi.org/10.1175/1520-0469(1994)051<2613:SOCMAC>2.0.CO;2.

Chen, S., M. K. Yau, and P. Bartello, 2018: Turbulence effects of collision efficiency and broadening of droplet size distribution in cumulus clouds. *J. Atmos. Sci.*, **75**, 203–217, https://doi.org/10.1175/JAS-D-17-0123.1.

Chillà, F., and J. Schumacher, 2012: New perspectives in turbulent Rayleigh–Bénard convection. *Eur. Phys. J. E*, **35**, 58, https://doi.org/10.1140/epje/i2012-12058-1.

Cooper, W. A., 1989: Effects of variable droplet growth histories on droplet size distributions. Part I: Theory. *J. Atmos. Sci.*, **46**, 1301–1311, https://doi.org/10.1175/1520-0469(1989)046<1301:EOVDGH>2.0.CO;2.

——, S. G. Lasher-Trapp, and A. M. Blyth, 2013: The influence of entrainment and mixing on the initial formation of rain in a warm cumulus cloud. *J. Atmos. Sci.*, **70**, 1727–1743, https://doi.org/10.1175/JAS-D-12-0128.1.

da Silva, C. B., J. C. R. Hunt, I. Eames, and J. Westerweel, 2014: Interfacial layers between regions of different turbulence intensity. *Annu. Rev. Fluid Mech.*, **46**, 567–590, https://doi.org/10.1146/annurev-fluid-010313-141357.

Deardorff, J. W., 1966: The counter-gradient heat flux in the lower atmosphere and in the laboratory. *J. Atmos. Sci.*, **23**, 503–506, https://doi.org/10.1175/1520-0469(1966)023<0503:TCGHFI>2.0.CO;2.

Desai, N., K. K. Chandrakar, K. Chang, W. Cantrell, and R. A. Shaw, 2018: Influence of microphysical variability on stochastic condensation in a turbulent laboratory cloud. *J. Atmos. Sci.*, **75**, 189–201, https://doi.org/10.1175/JAS-D-17-0158.1.

——, S. Glienke, J. Fugal, and R. A. Shaw, 2019: Search for microphysical signatures of stochastic condensation in marine boundary layer clouds using airborne digital holography. *J. Geophys. Res. Atmos.*, **124**, 2739–2752, https://doi.org/10.1029/2018JD029033.

Devenish, B. J., and Coauthors, 2012: Droplet growth in warm turbulent clouds. *Quart. J. Roy. Meteor. Soc.*, **138**, 1401–1429, https://doi.org/10.1002/qj.1897.

Ditas, F., R. A. Shaw, H. Siebert, M. Simmel, B. Wehner, and A. Wiedensohler, 2012: Aerosols-cloud microphysics-thermodynamics-turbulence: Evaluating supersaturation in a marine stratocumulus cloud. *Atmos. Chem. Phys.*, **12**, 2459–2468, https://doi.org/10.5194/acp-12-2459-2012.

Grabowski, W. W., and L.-P. Wang, 2013: Growth of cloud droplets in a turbulent environment. *Annu. Rev. Fluid Mech.*, **45**, 293–324, https://doi.org/10.1146/annurev-fluid-011212-140750.

——, and G. C. Abade, 2017: Broadening of cloud droplet spectra through eddy hopping: Turbulent adiabatic parcel simulations. *J. Atmos. Sci.*, **74**, 1485–1493, https://doi.org/10.1175/JAS-D-17-0043.1.

——, L. Thomas, and B. Kumar, 2022: Impact of cloud base turbulence on CCN activation: Single size CCN. *J. Atmos. Sci.*, **79**, 551–566, https://doi.org/10.1175/JAS-D-21-0184.1.

Hoffmann, F., S. Raasch, and Y. Noh, 2015: Entrainment of aerosols and their activation in a shallow cumulus cloud studied with a coupled LCM–LES approach. *Atmos. Res.*, **156**, 43–57, https://doi.org/10.1016/j.atmosres.2014.12.008.

Jeffery, C. A., J. M. Reisner, and M. Andrejczuk, 2007: Another look at stochastic condensation for subgrid cloud modeling: Adiabatic evolution and effects. *J. Atmos. Sci.*, **64**, 3949–3969, https://doi.org/10.1175/2006JAS2147.1.

Khairoutdinov, M. F., and D. A. Randall, 2003: Cloud resolving modeling of the ARM summer 1997 IOP: Model formulation, results, uncertainties, and sensitivities. *J. Atmos. Sci.*, **60**, 607–625, https://doi.org/10.1175/1520-0469(2003)060<0607:CRMOTA>2.0.CO;2.

Khvorostyanov, V. I., and J. A. Curry, 1999: Toward the theory of stochastic condensation in clouds. Part I: A general kinetic equation. *J. Atmos. Sci.*, **56**, 3985–3996, https://doi.org/10.1175/1520-0469(1999)056<3985:TTTOSC>2.0.CO;2.

Kogan, Y. L., 2006: Large-eddy simulation of air parcels in stratocumulus clouds: Time scales and spatial variability. *J. Atmos. Sci.*, **63**, 952–967, https://doi.org/10.1175/JAS3665.1.

Kolmogorov, A. N., 1941: The local structure of turbulence in incompressible viscous fluid for very large Reynolds numbers. *Dokl. Akad. Nauk SSSR*, **30**, 301–305.

Korolev, A. V., 1995: The influence of supersaturation fluctuations on droplet size spectra formation. *J. Atmos. Sci.*, **52**, 3620–3634, https://doi.org/10.1175/1520-0469(1995)052<3620:TIOSFO>2.0.CO;2.

——, and I. Mazin, 1993: Zones of increased and decreased droplet concentration in stratiform clouds. *J. Appl. Meteor.*, **32**, 760–773, https://doi.org/10.1175/1520-0450(1993)032<0760:ZOIADD>2.0.CO;2.

——, and I. P. Mazin, 2003: Supersaturation of water vapor in clouds. *J. Atmos. Sci.*, **60**, 2957–2974, https://doi.org/10.1175/1520-0469(2003)060<2957:SOWVIC>2.0.CO;2.

Krueger, S. K., 2020: Equilibrium droplet size distributions in a turbulent cloud chamber with uniform supersaturation. *Atmos. Chem. Phys.*, **20**, 7895–7909, https://doi.org/10.5194/acp-20-7895-2020.

Lasher-Trapp, S. G., W. A. Cooper, and A. M. Blyth, 2005: Broadening of droplet size distributions from entrainment and mixing in a cumulus cloud. *Quart. J. Roy. Meteor. Soc.*, **131**, 195–220, https://doi.org/10.1256/qj.03.199.

Levin, L. M., and Y. S. Sedunov, 1966: A kinetic equation describing microphysical processes in clouds. *Dokl. Akad. Nauk SSSR*, **170**, 323–326.

MacMillan, T., R. A. Shaw, W. H. Cantrell, and D. H. Richter, 2022: Direct numerical simulation of turbulence and microphysics in the pi chamber. *Phys. Rev. Fluids*, **7**, 020501, https://link.aps.org/doi/10.1103/PhysRevFluids.7.020501.

Magaritz-Ronen, L., M. Pinsky, and A. Khain, 2014: Effects of turbulent mixing on the structure and macroscopic properties of stratocumulus clouds demonstrated by a Lagrangian trajectory model. *J. Atmos. Sci.*, **71**, 1843–1862, https://doi.org/10.1175/JAS-D-12-0339.1.

Manton, M. J., 1979: On the broadening of a droplet distribution by turbulence near cloud base. *Quart. J. Roy. Meteor. Soc.*, **105**, 899–914, https://doi.org/10.1002/qj.49710544613.

Mazin, I. P., 1966: On temperature and humidity stratification in clouds. *Tr.* TsAO, **71**, 3–15.

——, and V. I. Smirnov, 1969: To the theory of cloud droplet size spectra formation due to stochastic condensation process. *Trudi CAO*, **89**, 92–94.

——, and V. M. Merkulovich, 2008: Stochastic condensation and its possible role in liquid cloud microstructure formation. *Some Problems of Cloud Physics: Collected Papers*, A. A. Ivanov et al., Eds., National Geophysical Committee, Russian Academy of Science, 217–267.

McGraw, R., and Y. Liu, 2006: Brownian drift-diffusion model for evolution of droplet size distributions in turbulent clouds. *Geophys. Res. Lett.*, **33**, L03802, https://doi.org/10.1029/2005GL023545.

Nair, V., T. Heus, and M. Van Reeuwijk, 2020: Dynamics of subsiding shells in actively growing clouds with vertical updrafts.

J. Atmos. Sci., **77**, 1353–1369, https://doi.org/10.1175/JAS-D-19-0018.1.

Narasimha, R., 1990: The utility and drawbacks of traditional approaches. *Lecture Notes in Physics,* J. L. Lumley, Ed., Vol. 357, *Whither Turbulence? Turbulence at the Crossroads*, Springer, 13–48.

Paluch, I. R., and C. A. Knight, 1984: Mixing and the evolution of cloud droplet size spectra in a vigorous continental cumulus. *J. Atmos. Sci.*, **41**, 1801–1815, https://doi.org/10.1175/1520-0469(1984)041<1801:MATEOC>2.0.CO;2.

——, and ——, 1986: Does mixing promote cloud droplet growth? *J. Atmos. Sci.*, **43**, 1994–1998, https://doi.org/10.1175/1520-0469(1986)043<1994:DMPCDG>2.0.CO;2.

Paoli, R., and K. Shariff, 2009: Turbulent condensation of droplets: Direct simulation and a stochastic model. *J. Atmos. Sci.*, **66**, 723–740, https://doi.org/10.1175/2008JAS2734.1.

Pinsky, M., A. Khain, and A. Korolev, 2016: Theoretical analysis of mixing in liquid clouds–Part 3: Inhomogeneous mixing. *Atmos. Chem. Phys.*, **16**, 9273–9297, https://doi.org/10.5194/acp-16-9273-2016.

Pope, S. B., 2000: *Turbulent Flows*. Cambridge University Press, 771 pp.

Prabhakaran, P., A. S. M. Shawon, G. Kinney, S. Thomas, W. Cantrell, and R. A. Shaw, 2020: The role of turbulent fluctuations in aerosol activation and cloud formation. *Proc. Natl. Acad. Sci. USA*, **117**, 16 831–16 838, https://doi.org/10.1073/pnas.2006426117.

Saito, I., T. Gotoh, and T. Watanabe, 2019: Broadening of cloud droplet size distributions by condensation in turbulence. *J. Meteor. Soc. Japan*, **97**, 867–891, https://doi.org/10.2151/jmsj.2019-049.

Sardina, G., F. Picano, L. Brandt, and R. Caballero, 2015: Continuous growth of droplet size variance due to condensation in turbulent clouds. *Phys. Rev. Lett.*, **115**, 184501, https://doi.org/10.1103/PhysRevLett.115.184501.

——, S. Poulain, L. Brandt, and R. Caballero, 2018: Broadening of cloud droplet size spectra by stochastic condensation: Effects of mean updraft velocity and CCN activation. *J. Atmos. Sci.*, **75**, 451–467, https://doi.org/10.1175/JAS-D-17-0241.1.

Shaw, R. A., 2003: Particle-turbulence interactions in atmospheric clouds. *Annu. Rev. Fluid Mech.*, **35**, 183–227, https://doi.org/10.1146/annurev.fluid.35.101101.161125.

Shawon, A. S. M., P. Prabhakaran, G. Kinney, R. A. Shaw, and W. Cantrell, 2021: Dependence of aerosol-droplet partitioning on turbulence in a laboratory cloud. *J. Geophys. Res. Atmos.*, **126**, e2020JD033799, https://doi.org/10.1029/2020JD033799.

Siebert, H., and R. A. Shaw, 2017: Supersaturation fluctuations during the early stage of cumulus formation. *J. Atmos. Sci.*, **74**, 975–988, https://doi.org/10.1175/JAS-D-16-0115.1.

Siewert, C., J. Bec, and G. Krstulovic, 2017: Statistical steady state in turbulent droplet condensation. *J. Fluid Mech.*, **810**, 254–280, https://doi.org/10.1017/jfm.2016.712.

Telford, J. W., and S. K. Chai, 1980: A new aspect of condensation theory. *Pure Appl. Geophys.*, **118**, 720–742, https://doi.org/10.1007/BF01593025.

Thomas, S., M. Ovchinnikov, F. Yang, D. van der Voort, W. Cantrell, S. K. Krueger, and R. A. Shaw, 2019: Scaling of an atmospheric model to simulate turbulence and cloud microphysics in the pi chamber. *J. Adv. Model. Earth Syst.*, **11**, 1981–1994, https://doi.org/10.1029/2019MS001670.

——, P. Prabhakaran, W. Cantrell, and R. A. Shaw, 2021: Is the water vapor supersaturation distribution Gaussian? *J. Atmos. Sci.*, **78**, 2385–2395, https://doi.org/10.1175/JAS-D-20-0388.1.

Turner, J. S., 1986: Turbulent entrainment: The development of the entrainment assumption, and its application to geophysical flows. *J. Fluid Mech.*, **173**, 431–471, https://doi.org/10.1017/S0022112086001222.

Twomey, S., 1977: The influence of pollution on the shortwave albedo of clouds. *J. Atmos. Sci.*, **34**, 1149–1152, https://doi.org/10.1175/1520-0469(1977)034<1149:TIOPOT>2.0.CO;2.

Wang, J., P. H. Daum, S. S. Yum, Y. Liu, G. I. Senum, M.-L. Lu, J. H. Seinfeld, and H. Jonsson, 2009: Observations of marine stratocumulus microphysics and implications for processes controlling droplet spectra: Results from the marine stratus/stratocumulus experiment. *J. Geophys. Res.*, **114**, D18210, https://doi.org/10.1029/2008JD011035.

Wang, S., Q. Wang, and G. Feingold, 2003: Turbulence, condensation, and liquid water transport in numerically simulated nonprecipitating stratocumulus clouds. *J. Atmos. Sci.*, **60**, 262–278, https://doi.org/10.1175/1520-0469(2003)060<0262:TCALWT>2.0.CO;2.

Warner, J., 1969: The microstructure of cumulus cloud. Part I. General features of the droplet spectrum. *J. Atmos. Sci.*, **26**, 1049–1059, https://doi.org/10.1175/1520-0469(1969)026<1049:TMOCCP>2.0.CO;2.

Yang, F., R. Shaw, and H. Xue, 2016: Conditions for superadiabatic droplet growth after entrainment mixing. *Atmos. Chem. Phys.*, **16**, 9421–9433, https://doi.org/10.5194/acp-16-9421-2016.

——, P. Kollias, R. A. Shaw, and A. M. Vogelmann, 2018: Cloud droplet size distribution broadening during diffusional growth: Ripening amplified by deactivation and reactivation. *Atmos. Chem. Phys.*, **18**, 7313–7328, https://doi.org/10.5194/acp-18-7313-2018.

——, M. Ovchinnikov, S. Thomas, A. Khain, R. McGraw, R. A. Shaw, and A. M. Vogelmann, 2022: Large-eddy simulations of a convection cloud chamber sensitivity to bin microphysics and advection. *J. Adv. Model. Earth Syst.*, **14**, e2021MS002895, https://doi.org/10.1029/2021MS002895.

Yau, M. K., and R. R. Rogers, 1996: *A Short Course in Cloud Physics*. 3rd ed. Elsevier, 304 pp.